Impurity-induced Raman scattering in CsBr and CsI

M. Buchanan, W. Bauhofer, and T. P. Martin
Max-Planck-Institut für Festkörperforschung, Stuttgart, Federal Republic of Germany
(Received 2 May 1974)

Measurements of the first-order impurity-induced Raman scattering in CsBr:I^- and CsI:Br^- are reported. Comparison is made with a corresponding phonon Green's-function calculation. Using known perfect-crystal shell-model parameters, only one additional parameter, the change in the longitudinal nearest-neighbor force constant, is needed to describe the dynamical properties of the defect and to fit the shape of the three independent Raman spectra with A_{1g}, E_g, and T_{2g} symmetry. Assumptions about the form of the terms giving rise to the Raman scattering permit the fitting of the relative intensities of these three spectra with one parameter.

I. INTRODUCTION

First-order Raman scattering is not allowed in pure crystals with CsCl structure since each ion is at a center of inversion. The addition of an impurity destroys the inversion symmetry of all lattice sites except the impurity site itself and first-order Raman scattering becomes possible. The impurity also destroys the translational symmetry of the lattice, breaking selection rules based on momentum conservation. Therefore, the first-order Raman spectrum of an impure crystal does not consist of a few discrete lines but is a continuum, reflecting in a complicated way the density of states of the perfect crystal and the frequency dependence of the eigenvectors of the imperfect crystal.

Measurements[1,2] and calculations[3,4] of the impurity-induced infrared absorption in cesium halides have been reported. The present Raman investigation complements the infrared absorption experiments in the following way. Only some odd-parity modes of vibration contribute to infrared absorption. The modes of vibration in which the displacement of the impurity is large are particularly important in infrared absorption spectra. On the other hand, only even modes of vibration contribute to Raman scattering. The motion of the impurity itself does not enter into the problem; therefore, all results are independent of the mass of the impurity.

Impurity-induced Raman scattering in alkali halides with NaCl structure has already been studied in some detail.[5-8] In the present work, we have chosen to examine alkali halides with CsCl structure. Specifically, results are presented for the complementary systems CsBr:I^- and CsI:Br^-. The data are analyzed by making an appropriate model Green's-function calculation.[9-11] Since detailed neutron scattering[12,13] and second-order Raman scattering[14] measurements have been made on CsBr and CsI, the phonons of the perfect crystal are well known. The analysis can, therefore, give reliable information about the defect-model force constants and the polarizability tensor expansion coefficients.

II. EXPERIMENTAL METHODS

The Raman measurements were made at room temperature using an argon laser and a Jarrel-Ash double monochromator. The data were processed using a photon counting system. A scattering geometry was used with the incident light propagating along the [001] crystallographic axis Z and the scattered light propagating in the [110] direction Y. The three independent Raman spectra, A_{1g}, E_g, and T_{2g}, can be determined by measuring the $Z(XX)Y$, $Z(XZ)Y$, and $Z(YX)Y$ spectra, where the symbols in the parentheses refer to the polarization of the exciting and the scattered light, respectively. Since there is an ambiguity in the definition of the E_g component, the reduction formulas should be written explicitly,

$$\begin{aligned} I[Z(XX)Y] &= I(A_{1g}) + I(E_g) + I(T_{2g}), \\ I[Z(XZ)Y] &= I(T_{2g}), \\ I[Z(YX)Y] &= 3I(E_g). \end{aligned} \tag{1}$$

The single crystals were grown from the melt, adding the desired impurity. A chemical analysis showed that the CsI crystal contained 13.8-at.% Br^-, and the CsBr crystal 6.2-at.% I^-. Since x-ray measurements of CsBr and CsI need very long exposure times, the orientations of the crystals were therefore determined using a method given by Maier.[15] This procedure is based on the fact that stress applied to a crystal surface of CsBr or CsI causes plastic deformations which mark the projections of the cubic axes on this surface. The birefringence caused by the punch patterns can easily be observed using crossed polarizers.

The results of the Raman measurements are shown in Figs. 1 and 2. In each figure, the pure-

cesium-halide spectrum is compared with the corresponding doped-crystal spectrum. The two curves are expected to be nearly identical for frequencies above the one-phonon cutoff. For the strongest spectrum, the Raman intensities of the pure and impure crystals were normalized to be approximately equal beyond this limiting frequency. This single normalization then fixes the relative intensities for the remaining two spectra.

III. CALCULATION

The calculation of the first-order impurity-induced Raman scattering in the CsCl structure has been previously discussed.[10,11] We repeat here the relevant equations.

The first-order impurity-induced Raman scattering per unit solid angle Ω is given by[9]

$$I(\omega,\omega';\Omega)=\frac{\omega^4\hbar}{2\pi^2c^3}\sum_{\alpha\alpha'}\sum_{\beta\beta'}\sum_{l\gamma}\sum_{l'\gamma'}n_\alpha n_{\alpha'}E_\beta E_{\beta'}P_{\alpha\beta,\gamma}(l)P_{\alpha'\beta',\gamma'}(l')\,n(\omega-\omega')\lim_{\epsilon\to0}\mathrm{Im}G_{\gamma\gamma'}(l,l';\omega^2-\omega'^2-i\epsilon)\,, \tag{2}$$

where ω and ω' are the frequencies of the incident and scattered light, $\vec{n}$ is the unit polarization vector of the scattered light, $\vec{E}$ is the incident field vector, $\underline{G}$ is the phonon Green's-function matrix of the imperfect crystal, and $n(\omega-\omega')$ is the thermal occupation number. In this expression, the polarizability tensor has been expanded in the ionic displacements $\vec{u}(l)$,

$$P_{\alpha\beta}=P^0_{\alpha\beta}+\sum_{l\gamma}P_{\alpha\beta,\gamma}u_\gamma(l)+\cdots, \tag{3}$$

with the term linear in $\vec{u}(l)$ giving rise to the first-order Raman scattering. In the perfect crystal, this term is zero by symmetry, but in a crystal with defects, neighbors of the defect no longer possess inversion symmetry. We shall assume that this sum need only be taken over first neighbors of the defect, because of the rather rapid drop-off with distance of the terms which give rise to the dependence of $\underline{P}$ on the ionic displacement.

The Green's-function matrix $\underline{G}$ of the imperfect crystal can be written in terms of the Green's function $\underline{G}^0$ of the perfect crystal and a matrix $\underline{\Gamma}$ describing the defect,

$$\underline{G}=\underline{G}^0(\underline{I}+\underline{\Gamma}\underline{G}^0)^{-1}\,. \tag{4}$$

We assume that $\underline{\Gamma}$ has nonzero elements only in the space of the impurity and its first neighbors.

It is then convenient to transform from Cartesian coordinates to the cubic symmetry coordinates of the first neighbors, since the assumptions on both $\underline{P}$ and $\underline{\Gamma}$ restrict our problem to this space. Group-theoretical considerations then show that only four of these cubic symmetry coordinates are Raman active: one A_{1g}, one E_g, and two T_{2g}. These coordinates are pictured in Ref. 10.

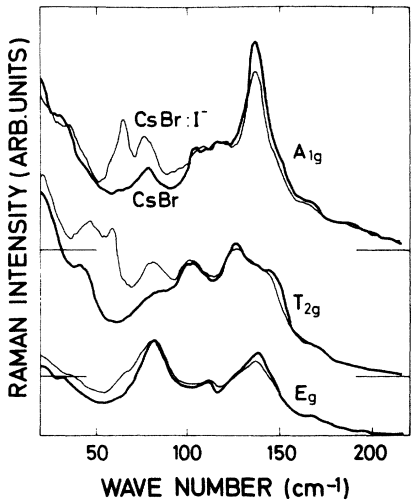

FIG. 1. Measured room-temperature Raman spectra of pure CsBr (heavy lines) and of CsBr:I^- (light lines). The difference between these two spectra is due to impurity-induced first-order Raman scattering.

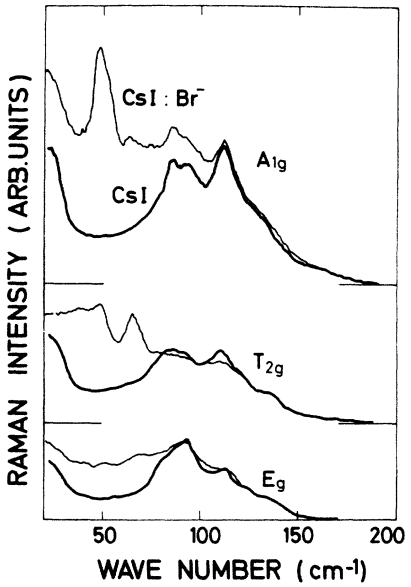

FIG. 2. Measured room-temperature Raman spectra of pure CsI (heavy lines) and of CsI:Br^- (light lines). The difference between these two spectra is due to impurity-induced first-order Raman scattering.

In the cubic symmetry space, then, we may write,

$$\begin{aligned}
\Gamma(A_{1g}) &= -\Delta A\,,\\
\Gamma(E_g) &= -\Delta B\,,\\
\Gamma_{11}(T_{2g}) &= -\tfrac{1}{3}(\Delta A + 2\Delta B)\,,\\
\Gamma_{12}(T_{2g}) &= -\tfrac{1}{3}\sqrt{2}\Delta A\,,\\
\Gamma_{22}(T_{2g}) &= -\tfrac{1}{3}(2\Delta A + \Delta B)\,,
\end{aligned} \tag{5}$$

where ΔA and ΔB are the change of the longitudinal and transverse first-neighbor force constants from their perfect crystal values, A and B; and

$$\begin{aligned}
I(A_{1g}) &= C^2(A_{1g})G(A_{1g})\,,\\
I(E_g) &= C^2(E_g)G(E_g)\,,\\
I(T_{2g}) &= C^2[T_{2g}(1)]G_{11}(T_{2g})\\
&\quad + 2C[T_{2g}(1)]C[T_{2g}(2)]G_{12}(T_{2g})\\
&\quad + C^2[T_{2g}(2)]G_{22}(T_{2g})\,,
\end{aligned} \tag{6}$$

where

$$\begin{aligned}
C(A_{1g}) &= \sqrt{2}(P_{xx,x} + 2P_{xx,y})\,,\\
C(E_g) &= P_{xx,x} - P_{xx,y}\,,\\
C[T_{2g}(1)] &= \sqrt{6}P_{xy,z}\,,\\
C[T_{2g}(2)] &= 4\sqrt{3}P_{xy,x}\,.
\end{aligned} \tag{7}$$

The numerical constants in Eq. (7) arise from the definitions of the experimental intensities $I(A_{1g})$, $I(E_g)$, and $I(T_{2g})$ in terms of the measured quantities, and of the Green's functions in normalized symmetry coordinates. The four $P_{\alpha\beta,\gamma}$ that appear are the only distinct ones as a result of symmetry considerations. They are defined for the first neighbor of the defect in the [111] direction.

To interpret the meaning of the $P_{\alpha\beta,\gamma}$'s, and to be able to make assumptions that give relations between them, we look more closely at their meaning within the framework of the shell model.

Let us first write the Hamiltonian of the perturbed crystal,

$$H = H^0 + H'\,. \tag{9}$$

H^0 is the Hamiltonian of the perfect crystal and H' contains the changes as a result of the defect. Both can be expanded in Taylor series in the degrees of freedom of the crystal, $\vec{u}$, the core displacements, and $\vec{w}$, the relative shell-core displacements. The quadratic terms in H^0 give the perfect crystal frequencies and eigenvectors; the quadratic terms in H' give the perturbation of these solutions; and the cubic terms in H' permit first-order Raman scattering. Since the changes in interionic force constants dominate the changes in harmonic lattice dynamics for these crystals, the effect of H' on this part of the problem is well treated by Eq. (4) used in the rigid-ion approximation; only the terms quadratic in $\vec{u}$, the ionic displacement, are important. For the Raman scattering, however, we require cubic terms that are at least quadratic in $\vec{w}$, since the $\vec{w}$'s represent the electronic degrees of freedom and are required to give the coupling between the light and the lattice at optical frequencies.

In the shell model, the polarizability is given by

$$\underline{P} = \sum_{ll'} Y_l \Phi^{-1}_{ww}(ll') Y_{l'}\,, \tag{10}$$

where Φ_{wu} is the second derivative of the short range part of H with respect to $\vec{w}$, and Y_l is the shell charge of ion l. We may expand Φ^{-1}_{ww} in a series to get the form of the first-order term $P^1_{\alpha\beta}$,

$$\begin{aligned}
P^1_{\alpha\beta} &= \sum_l P_{\alpha\beta,\gamma}(l)u_\gamma(l)\\
&= -\sum_{\substack{ll'\\LL'\\ab}} Y_l \Phi^{-1}_{ww}\begin{pmatrix} l & L\\ \alpha & a\end{pmatrix}\left[\sum_{L''\gamma}\Phi_{wwu}\begin{pmatrix} LL' & L''\\ ab & \gamma\end{pmatrix}u_\gamma(L'')\right]\Phi^{-1}_{ww}\begin{pmatrix} L' & l\\ b & \beta\end{pmatrix}Y_l\,,
\end{aligned} \tag{11}$$

where Φ_{ww} is now the second derivative with respect to $\vec{w}$ of the *harmonic* part of H, and the Φ_{wwu} are third derivatives, the coefficients of the cubic terms in H' that give Raman scattering. The summation over L, L', and L'' is restricted to the space of the defect and its first neighbors, and also at least two of L, L', L'' must refer to the same ion. We have neglected the terms in $\Phi_{www'}$ as for these crystals $|\vec{w}| \ll |\vec{u}|$.

Φ_{ww} is to a good approximation diagonal, as the shell-core force constant is much larger than the first-neighbor force constant; the only important terms in Eq. (11) are those where $l = L$, $l' = L'$, $\alpha = a$, and $\beta = b$. The elements of Φ^{-1}_{ww} are proportional to the polarizabilities of the defect or the first neighbors in the perturbed harmonic system. There are three kinds of contributions to $\underline{P}^1$: the self-modulation of the polarizability of the first-neighbor ions as a result of their motion against the defect ($L = L'$ = first neighbor), cross terms which represent a sort of bond polarizability ($L = 0$, L' = first neighbor), and the term representing the

change of polarizability of the defect due to the motions of the first neighbors ($L = L' = 0$). This last term is expected to be the most important as the polarizability of the negative ions is larger.

We now assume that the part of H' that gives rise to Raman scattering can be written as a central potential $\sum_l \phi(|\vec{r}_{0l}|)$, a function of

$$\vec{r}_{0l} = \vec{R}_0 + (\vec{u}_0 + \vec{w}_0) - (\vec{u}_l + \vec{w}_l),$$

where 0 refers to the defect and l to the first neighbors. Such a term represents a shell-shell coupling between the defect and its neighbors, which might be expected to give the largest contribution because of the importance of such couplings in the harmonic problem. The various derivatives Φ_{uwu} required in Eq. (11) can then be written in terms of only two constants ϕ'' and ϕ''', the second and third derivatives of ϕ with respect to r^2, evaluated at the equilibrium separation $\vec{R}_0 = a[111]$. Then, to within a common constant which depends on the harmonic polarizabilities and the shell charges as in Eq. (11), the set of Eq. (7) becomes,

$$\begin{aligned} C(A_{1g}) &= \sqrt{2}(5\phi'' + 6a^2\phi'''), \\ C(E_g) &= (2\phi''), \\ C[T_{2g}(1)] &= \sqrt{6}(2a^2\phi'''), \\ C[T_{2g}(2)] &= 4\sqrt{3}(\phi'' + 2a^2\phi'''). \end{aligned} \tag{12}$$

The relative values of the C^2's are plotted in Fig. 3 as functions of $x = 2a^2\phi'''/\phi''$. The values of ϕ'' are not well determined by the perturbed harmonic values, since different terms in H' are important for the lattice dynamics and for the Raman scattering.

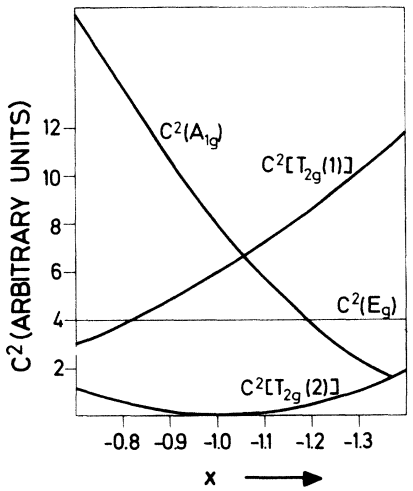

FIG. 3. Relative intensities of the contributions of the four symmetry coordinates under the assumption of a central potential. The abscissa is the ratio $x = 2a^2\phi'''/\phi''$, where ϕ'' and ϕ''' are second and third derivatives of the potential responsible for the defect-induced scattering.

We comment that the form of this result is rather more general than might appear from the above discussion; the important assumptions are only that the polarizability can be written as a second derivative (with respect to some electronic degrees of freedom) of some potential, and that this potential, or rather the part of it that can give rise to Raman scattering, can be written as a central potential as a function of differences of the first-neighbor coordinates and the defect coordinates. It is not essential that Φ_{wu} be diagonal, nor that ϕ represent only shell-shell coupling; ϕ may be a sum of central potentials, that is, functions of $|\vec{R}_0 + \vec{u}_0 - (\vec{u}_l + \vec{w}_l)|$, of $|\vec{R}_0 + (\vec{u}_0 + \vec{w}_0) - \vec{u}_l|$, or of $|\vec{w}_l|$ may be added. This generalization would change the definitions of the two constants that appear in Eq. (12); they would then involve summations over several terms, including coefficients as in Eq. (11). However, the final form of Eq. (12) would be the same.

IV. RESULTS AND DISCUSSION

The frequencies and eigenvectors for the perfect crystal have been calculated for 1771 $\vec{q}$-values in $\frac{1}{48}$th of the Brillouin zone, using for CsI the eleven-parameter model of Bührer and Hälg[12] and for CsBr the model of Daubert *et al.*[13] Both models are for 300 °K. The imaginary parts of the Green's functions were calculated by forming a histogram with 100 bins; the real parts were found by a Kramers-Kronig transformation. The force constant changes ΔA and ΔB were varied to obtain the best fit to experiment.

A good fit to experiment was obtained for CsI:Br^- with $\Delta A = -\frac{1}{2}A$, $\Delta B = 0$, and for CsBr:I^- with $\Delta A = \frac{1}{4}A$, $\Delta B = 0$. Because the E_g spectra (which depend most sensitively on ΔB) were rather weak and the experimental errors therefore high, ΔB was chosen to be zero for simplicity. The unperturbed E_g spectra agree reasonably well with experiment.

In the case of CsI, ΔA was chosen to give the correct frequency for the strong A_{1g} peak at 49 cm^{-1}, which does not appear in the unperturbed calculation. For CsBr, the unperturbed A_{1g} spectrum agrees in shape rather well with experiment, but the frequency of the strongest peak is lower than that measured. Since the lattice-dynamical model for this system was fitted to an unusually large number of measured frequencies, including off-symmetry $\vec{q}$ values, it seems unlikely that the model is predicting frequencies wrongly; therefore, ΔA was chosen to give the best frequency agreement with experiment.

Since no infrared measurements exist for the

systems considered here, it is not possible to compare these values of ΔA with those obtained in other calculations, however, their sizes seem reasonable by comparison with those obtained for related systems.[1,3]

One fortunate result of the calculation of the T_{2g} spectra is that the two T_{2g} coordinates lead to peaks in different frequency regimes, $T_{2g}(1)$ peaking approximately where the experimental spectra do, and $T_{2g}(2)$ peaking at lower frequencies for both systems and for all choices of Γ investigated. Thus, we can say that $C^2[T_{2g}(2)]$ must be much less than $C^2[T_{2g}(1)]$, allowing for uncertainties in the shape of $I(T_{2g})$ due to errors in subtraction. Thus, we have, in effect, four pieces of information on the intensities from the three experimental spectra. If we make the central potential assumption, we must fit four intensities with two parameters. Inspection of Fig. 3 shows that the A_{1g} and $T_{2g}(1)$ intensities cross over in the region of zero intensity for $T_{2g}(2)$ and that they are both stronger than $C^2(E_g)$ in this region. A value of $x=-0.93$ for CsI:Br$^-$ and of $x=-1.09$ for CsBr:I$^-$ gives the experimentally observed intensities for $I(A_{1g})$, $I(E_g)$, and $I(T_{2g})$ correctly with the contribution of the $T_{2g}(2)$ coordinate negligibly small, as required. Figures 4 and 5 show the calculated curves for the force constant changes and x values above, compared with experiment; in addition, the small contribution of $T_{2g}(2)$ multiplied by 50 is shown to display its frequency dependence.

The agreement in shape and intensity is seen to be excellent. The poorer agreement for $I(E_g)$ for CsBr:I$^-$ is not felt to be significant since the experimental uncertainty is particularly large. The experimental peaks are broader and weaker than those calculated using a harmonic model for low impurity concentration. Anharmonic interaction of room temperature phonons could easily account for a broadening of about 5 cm^{-1}, and the high impurity concentration present in the samples can give a non-negligible inhomogeneous contribution to the experimental linewidths since the impurities may have different environments. There may, in addition, be some background due to changes in the second-order spectra in the doped crystals (see, for example, the 140-cm^{-1} peak in the A_{1g} spectrum in Fig. 1), and from interference between first- and second-order spectra, which could become important at such concentrations.

V. CONCLUSIONS

The first-order impurity-induced Raman scattering has been measured and calculated for the sys-

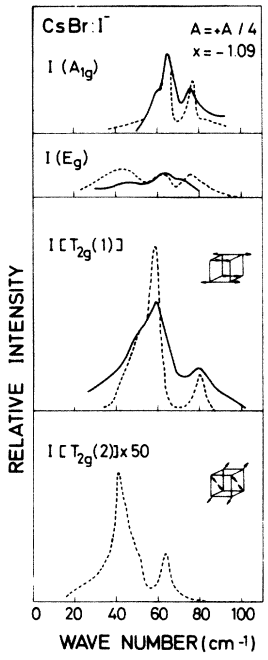

FIG. 4. Experimental (solid lines) and calculated (dashed lines) room-temperature Raman spectra for CsBr:I$^-$. The two T_{2g} symmetry coordinates have been indicated. The measured and calculated contribution to the Raman intensities from one of these symmetry coordinates, $T_{2g}(2)$, is very small.

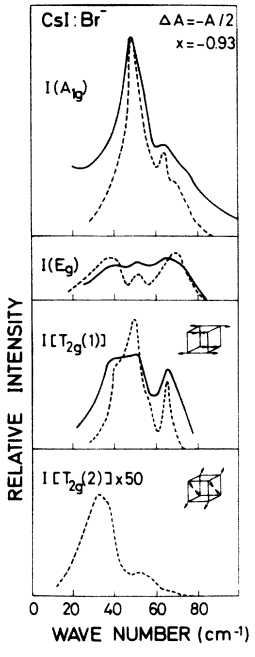

FIG. 5. Experimental (solid lines) and calculated (dashed lines) room-temperature Raman spectra for CsI:Br$^-$. The two T_{2g} symmetry coordinates have been indicated. The measured and calculated contribution to the Raman intensities from one of these symmetry coordinates, $T_{2g}(2)$, is very small.

tems CsBr:I^- and CsI:Br^-, with excellent agreement. The shape of the three independent Raman spectra for both systems can be fit with a single parameter, the change of the longitudinal first-neighbor force constant. As expected from the ionic radii, the system of I^- as an impurity in CsBr requires an increase of this force constant and Br^- in CsI requires a decrease. This force-constant change leads to a marked perturbation of the A_{1g} spectrum for CsI:Br^-, but rather small changes in the other spectra. We may conclude that the perfect crystal-phonon models determined using only neutron-measured eigenfrequencies yield realistic eigenvectors as a result of the good fit to the Raman measurements.

The intensities of the measured Raman spectra show several unusual properties. The T_{2g} spectrum predominates in CsBr:I^-, the A_{1g} spectrum in CsI:Br^-. In addition, for both systems, only one T_{2g} first-neighbor symmetry coordinate appears to contribute appreciably to the Raman scattering. The relative intensities of the spectra, including these unusual properties, can be determined with only one parameter if a central potential is assumed to describe the lowest-order nonlinear terms arising from the introduction of the defect. In addition, this parameter has nearly the same value for the two systems considered.

ACKNOWLEDGMENT

The authors are grateful to Dr. R. M. Martin for a critical reading of the manuscript.

[1]W. Prettl and E. Siep, Phys. Status. Solidi 44, 759 (1971).
[2]C. R. Becker, Solid State Commun. 9, 13 (1971).
[3]T. P. Martin, J. Phys. C 4, 2269 (1971).
[4]P. N. Ram and Bal K. Agrawal, Solid State Commun. 10, 1111 (1972).
[5]R. T. Harley, J. B. Page, C. T. Walker, Phys. Rev. B 3, 1365 (1971).
[6]G. P. Montgomery, W. R. Fenner, M. V. Klein, and T. Timusk, Phys. Rev. B 5, 3343 (1972).
[7]G. P. Montgomery, M. V. Klein, B. N. Ganguly, and R. F. Wood, Phys. Rev. B 6, 4047 (1972).
[8]W. Möller and R. Kaiser, Phys. Status Solidi B 50, 155 (1972).
[9]N. X. Xinh, A. A. Maradudin, and R. A. Coldwell-Horsfall, J. Phys. 26, 717 (1965).
[10]T. P. Martin, J. Phys. C 5, 493 (1972).
[11]P. N. Ram and B. K. Agrawal, Phys. Status Solidi B 55, 729 (1973).
[12]W. Bührer and W. Hälg, Phys. Status Solidi B 46, 679 (1971).
[13]J. Daubert, H. Jex, and M. Müllner, Phys. Status Solidi B 57, 477 (1973).
[14]B. S. Agrawal, R. D. Kirby, and J. R. Hardy (unpublished).
[15]K. Maier, J. Cryst. Growth 6, 111 (1969).